Least Squares Natural Migration of Back-scattered Surface Waves and Polarity Analysis

Zhaolun Liu[1]
[1]King Abdullah University of Science and Technology (KAUST)

ABSTRACT

The natural inversion method of backscattered surface waves is studied in this project. I give the conjugate gradient (CG) algorithm and compare its computational workload with that of the inverse of Hessian method. The CG algorithm needs much more computational workload than the inverse of Hessian method. Then, I show the polarity change in my implement of natural migration, and give the polarity analysis from the migration equation. The results of analysis demonstrates the polarity of final image changes when the source-receiver pair is at different side of a fault. But it still needs more works to study the polarity of the natural migration of surface waves.

INTRODUCTION

The scattered surface wave generated by strong heterogeneity of shallow subsurface is often seen as noise in seismic reflection exploration (Blonk et al., 1995; Ernst et al., 2002). Actually, we can use the backscattered surface wave to image the near-surface heterogeneity (Snieder, 1986; Riyanti, 2005; Yu et al., 2014).

The relations between model perturbation $\mathbf{m}$ and backscattered surface waves $\mathbf{d}$ can be linearized by Born approximation $\mathbf{d} = \mathbf{L}\mathbf{m}$, where $\mathbf{L}$ is the forward modeling operator (Snieder, 1986; Tanimoto, 1990). To get the model perturbation $\mathbf{m}$, Riyanti (2005) used an iterative optimization method to approximate the solution, and Snieder (1986) and Yu et al. (2014) applied the adjoint of the forward modeling operator $\mathbf{L}^\dagger$ to backscattered data to obtain the migration image.

Recently, AlTheyab et al. (2015c) introduced the natural migration (NM) method to image the near-surface heterogeneity. Compared to the methods introduced above, there are two main advantages of NM method. One is that the NM method does not base on the Born approximation and estimates the Green's function at the geophone instead of calculating the Green's function based on an assumed background model. Another is that the NM method can be implemented without a velocity model. AlTheyab et al. (2015c) has shown the image of USArray and Long Beach passive data by using the NM method.

The NM seems to migrate some artifacts due to recording geometry and bad illumination (AlTheyab et al., 2015a). AlTheyab et al. (2015b) has applied the inverse of Hessian method to do natural inversion. This project tries to use the conjugate gradient (CG) method to solve this problem and compare its result with the inverse of Hessian method.

In the following section, I begin by overview of the theory of two least-square implement methods, CG method and the inverse of Hessian method. Then, I will show the polarity change that exists in my implement by a one-fault model. Finally, I will analyze the polarity of image from the migration equation.

LEAST SQUARE NATURAL MIGRATION

The natural migration equation can be expressed as (AlTheyab et al., 2015b),

$$\mathbf{m} = \mathbf{L}^\dagger \mathbf{d} \tag{1}$$

where $\mathbf{m}$ is the perturbation model; $\mathbf{L}$ is the forward-modeling operator, and $\mathbf{d}$ is the vector containing the scattered events.

In this section, we try to see this migration problem as an inversion problem, and analyze two implements.

The conjugate gradient method

To obtain the perturbation model $\mathbf{m}$, I turn to the CG method to solve the system of linear equations $\mathbf{L}\mathbf{m} = \mathbf{d}$

instead of just applying the migration equation 7. The CG algorithm is shown in algorithm 1. For each iteration, it needs two modeling (line 5 and line 8 in algorithm 1) and one migration (line 14).

Algorithm 1 The Conjugate Gradient Algorithm

1: initial $\mathbf{m}_0 = 0$;
2: $\mathbf{g}_1 \leftarrow \mathbf{L}^T\mathbf{d}$;
3: $\mathbf{p}_1 \leftarrow -\mathbf{g}_1$;
4: **for** each i in [1,$MaxIterationNo$] **do**
5: $\mathbf{res} = \mathbf{L}\mathbf{p}_i$;
6: $\alpha_i \leftarrow -(\mathbf{g}_i^T\mathbf{p}_i)/(\mathbf{res}^T\mathbf{res})$;
7: $\mathbf{m}_{i+1} \leftarrow \mathbf{m}_i + \alpha_i\mathbf{p}_i$;
8: $\mathbf{data}_{i+1} = \mathbf{L}\mathbf{m}_{i+1}$;
9: $\mathbf{data}_{\mathbf{res}} = \mathbf{data}_{i+1} - \mathbf{data}_{obs}$;
10: **if** $\mathbf{data}_{\mathbf{res}} < \delta$ **then**
11: break;
12: **end if**
13: mute the transmitted wave for $\mathbf{data}_{\mathbf{res}}$;
14: $\mathbf{g}_{i+1} \leftarrow \mathbf{L}^T\mathbf{data}_{\mathbf{res}}$;
15: **if** $mod(i, N) == 0$ **then**
16: $\beta_i \leftarrow 0$;//reset the direction to the steepest descent direction
17: **else**
18: $\beta_i \leftarrow (\mathbf{g}_{i+1}^T\mathbf{g}_{i+1})/(\mathbf{g}_i^T\mathbf{g}_i)$; //Fletcher-Reeves CG method
19: **end if**
20: $\mathbf{p}_{i+1} \leftarrow -\mathbf{g}_{i+1} + \beta_i\mathbf{p}_i$
21: **end for**

The inverse of Hessian method

To implement the least-squares solution, another method is to apply the inverse of Hessian to the migration equation 7, $\mathbf{m} = \mathbf{H}^{-1}\mathbf{L}^\dagger\mathbf{d}$, where the Hessian matrix is defined as $\mathbf{H} = \mathbf{L}^\dagger\mathbf{L}$.

$\mathbf{L}(\mathbf{g}|\mathbf{x}'|\mathbf{s})$ can be expressed as $2\omega^2 W(\omega)G(\mathbf{g}|\mathbf{x}')G(\mathbf{x}'|\mathbf{s})$, where, $\mathbf{g}$ and $\mathbf{s}$ represent the position of geophone and source; $\mathbf{x}'$ represent the position of model point; ω is the angular frequency; G is the Green's function. So, the Hessian can be expressed as,

$$\mathbf{H}(\mathbf{x}|\mathbf{x}') = \sum_{\mathbf{s},\mathbf{g},\omega} 4\omega^4 A(\omega)G(\mathbf{g}|\mathbf{x})^*G(\mathbf{x}|\mathbf{s})^*G(\mathbf{g}|\mathbf{x}')G(\mathbf{x}'|\mathbf{s}) \tag{2}$$

where $A = W^*(\omega)W(\omega)$. Each column of Hessian can be seen as the point-scatterer response in the migration image, and $\mathbf{x}'$ in equation 2 is the point-scatterer position.

The inverse of Hessian can be approximated by Singular Value Decomposition (SVD) method,

$$\mathbf{H} \overset{\text{def}}{=} \mathbf{U}\mathbf{W}\mathbf{V}^\dagger \tag{3}$$

$$\mathbf{H}^{-1} \approx \mathbf{V}\mathbf{S}\mathbf{U}^\dagger \tag{4}$$

where $\mathbf{U}$ and $\mathbf{V}$ are unitary matrices; $\mathbf{W}$ is a rectangular matrix with singular values at diagonal entries; $\mathbf{S}$ is the pseudo-inverse of matrix $\mathbf{W}$.

From the equation 2, we can see that it needs only one migration to calculate the Hessian, which means it is much cheaper than the iterative CG method.

POLARITY PROBLEM IN MY IMPLEMENT

In this section, I will use a one-fault model to show the polarity change in my implement, and then try to analyze this problem in theory.

A one-fault model

The one -fault model we used is shown in figure 1. The P-wave velocity is 1000 m/s on the left side and 1400 m/s on the right side. The S-wave velocity is calculated by $V_s = V_p/\sqrt{3}$. The density is constant with the value of 2.0 km/m^3. The fault is located at x= 122 m with the depth of 0 m. There are totally 301 sources and receivers on the surface with the spacing of 1 m. I used the 2D staggered-grid finite-difference forward modeling of isotropic elastic wave-equation (Virieux, 1986) with a free-surface boundary condition (Gottschämmer and Olsen, 2001) to generate the Rayleigh wave.

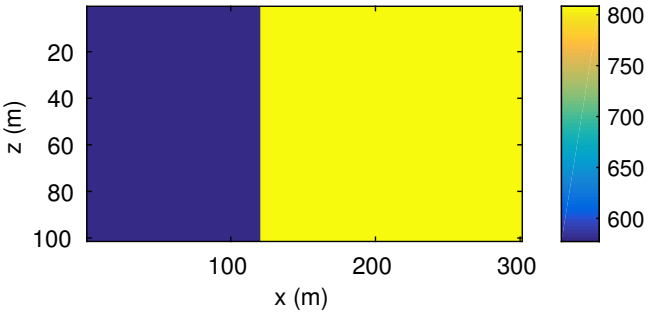

Figure 1: The shear velocity for a one-fault model, where the fault is located at $x = 122$ m.

Figure 2 shows the NM image for each shot, where the red dash line shows the position of fault; the stars show the position of each shot; the black arrow shows the polarity change when the source is at different sides of the fault.

Polarity analysis from the migration equation

I will try to think about this problem from the migration equation 7. The expression of the kernel is,

$$\mathbf{L}(\mathbf{g}|\mathbf{x}'|\mathbf{s})^\dagger = 2\omega^2 W^*(\omega)G(\mathbf{g}|\mathbf{x}')^*G(\mathbf{x}'|\mathbf{s})^* \tag{5}$$

The data we obtain can be expressed as the convolution between the source wavelet and the Green's function,

$$\mathbf{d}(\mathbf{g}|\mathbf{s}) = W(\omega)G(\mathbf{g}|\mathbf{s}) \tag{6}$$

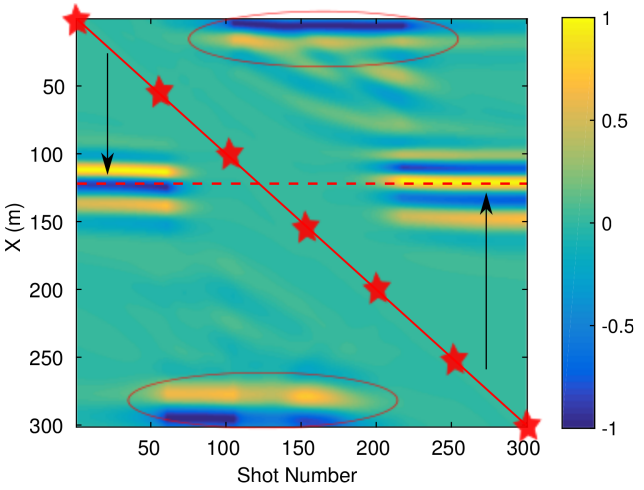

Figure 2: The NM image for each shot, where the red dash line shows the position of fault; the stars show the position of each shot; the black arrow shows the polarity change when the source is at different sides of the fault (the red ellipses show the image of the boundary due to the lack of visible backscattered waves near the source).

Then we can do migration by the following migration equation,

$$\begin{aligned} m(\mathbf{x}') &= \mathbf{L}(\mathbf{g}|\mathbf{x}'|\mathbf{s})^{\dagger}\mathbf{d}(\mathbf{g}|\mathbf{s}) \\ &= \sum_{\mathbf{s},\mathbf{g},\omega} 2\omega^2 W^*(\omega)G(\mathbf{g}|\mathbf{x}')^*G(\mathbf{x}'|\mathbf{s})^*W(\omega)G(\mathbf{g}|\mathbf{s}) \\ &= \sum_{\mathbf{s},\mathbf{g},\omega} 2\omega^2 A(\omega)G(\mathbf{g}|\mathbf{x}')^*G(\mathbf{x}'|\mathbf{s})^*G(\mathbf{g}|\mathbf{s}) \end{aligned} \quad (7)$$

where $A = W^*(\omega)W(\omega)$.

Two-side situation

Now we use a fault model in figure 3 to show the implement of migration. For the left source-receiver pair (the source and receiver are at the same position), we can calculate its migration image,

$$m_l(\mathbf{x}') = \sum_{\omega} 2\omega^2 A(\omega)G_l(\mathbf{g}_l|\mathbf{x}')^*G_l(\mathbf{x}'|\mathbf{s}_l)^*G_l(\mathbf{g}_l|\mathbf{s}_l) \quad (8)$$

Then, by using the same wavelet, we can obtain the migration image for the right source-receiver pair,

$$m_r(\mathbf{x}') = \sum_{\omega} 2\omega^2 A(\omega)G_r(\mathbf{g}_r|\mathbf{x}')^*G_r(\mathbf{x}'|\mathbf{s}_r)^*G_r(\mathbf{g}_r|\mathbf{s}_r) \quad (9)$$

By comparison of equation (8) and (9), I claim that if the distances between the fault and source-receiver for both sides are set appropriately, the Green's functions $G_l(\mathbf{g}_l|\mathbf{x}')(= G_l(\mathbf{x}'|\mathbf{s}_l))$ and $G_r(\mathbf{g}_r|\mathbf{x}')$ $(= G_r(\mathbf{x}'|\mathbf{s}_r))$ should be the same without the consideration of geometry spreading (this is the assumption for the following discussion). How about the remaining Green's function term? Obviously, there are two option, the same or reverse and I claim that they should be reverse, $G_l(\mathbf{g}_l|\mathbf{s}_l) = -G_r(\mathbf{g}_r|\mathbf{s}_r)$. So, the image should be reverse, $m_l(\mathbf{x}') = -m_r(\mathbf{x}')$.

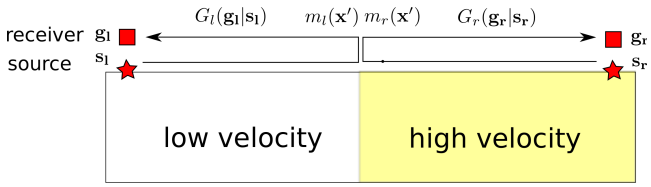

Figure 3: The schematic diagram that shows the source-receiver pairs at two sides of a fault.

One-side situation with velocity reverse

Now we are going to consider one-side situation shown in figure (4) but the velocity is reverse compared to that in figure (3). The migration image can be expressed as,

$$m'_l(\mathbf{x}') = \sum_{\omega} 2\omega^2 A(\omega)G'_l(\mathbf{g}'_l|\mathbf{x}')^*G'_l(\mathbf{x}'|\mathbf{s}'_l)^*G'_l(\mathbf{g}'_l|\mathbf{s}'_l) \quad (10)$$

By comparison between equation (8) and (10), I claim that if the distances between the fault and source-receiver at one side but with velocity reverse are set appropriately, the Green's functions $G_l(\mathbf{g}_l|\mathbf{x}')(= G_l(\mathbf{x}'|\mathbf{s}_l))$ and $G'_l(\mathbf{g}'_l|\mathbf{x}')$ $(= G'_l(\mathbf{x}'|\mathbf{s}'_l))$ should be the same. How about the remaining Green's function term? I also claim that they should be reverse, $G_l(\mathbf{g}_l|\mathbf{s}_l) = -G'_l(\mathbf{g}'_l|\mathbf{s}'_l)$. So, the image should be reverse, $m_l(\mathbf{x}') = -m'_l(\mathbf{x}')$.

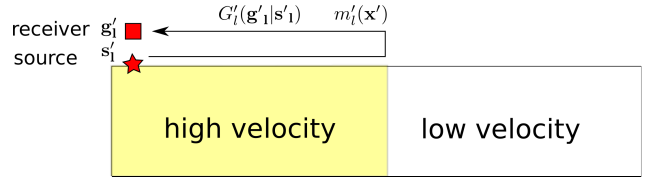

Figure 4: The schematic diagram that shows the source-receiver pair at one side of a fault with the velocity reverse compared to figure (3).

DISCUSSION

From the polarity analysis, it seems that the polarity should change when the source is at different sides of a fault. Actually, we can see the polarity change in the backscattered waves when source is at different sides of the fault (shown in figure 5), which leads to the polarity changes at the final image (shown in figure 6).

ACKNOWLEDGEMENTS

I would like to thank Professor Gerard Schuster, Abdullah AlTheyab and Lei Fu for their constructive comments and helpful discussion.

REFERENCES

AlTheyab, A., , F. Lin, and G. Schuster, 2015a, Imaging near-surface heterogeneities by natural migration of back-scattered surface waves: Geophysical Journal International.

———, 2015b, Natural inversion of scattered surface waves with application to rayleigh waves in long-beach passive data.

AlTheyab, A., E. Workman, F. Lin, and G. Schuster, 2015c, Imaging near-surface heterogeneities by natural migration of back-scattered surface waves: Presented at the 77th EAGE Conference and Exhibition-Workshops.

Blonk, B., G. C. Herman, and G. G. Drijkoningen, 1995, An elastodynamic inverse scattering method for removing scattered surface waves from field data: Geophysics, **60**, 1897–1905.

Ernst, F. E., G. C. Herman, and A. Ditzel, 2002, Removal of scattered guided waves from seismic data: Geophysics, **67**, 1240–1248.

Gottschämmer, E., and K. Olsen, 2001, Accuracy of the explicit planar free-surface boundary condition implemented in a fourth-order staggered-grid velocity-stress finite-difference scheme: Bulletin of the Seismological Society of America, **91**, 617–623.

Riyanti, C. D., 2005, Modeling and inversion of scattered surface waves: TU Delft, Delft University of Technology.

Snieder, R., 1986, 3-d linearized scattering of surface waves and a formalism for surface wave holography: Geophysical Journal International, **84**, 581–605.

Tanimoto, T., 1990, Modelling curved surface wave paths: membrane surface wave synthetics: Geophysical Journal International, **102**, 89–100.

Virieux, J., 1986, P-sv wave propagation in heterogeneous media: Velocity-stress finite-difference method: Geophysics, **51**, 889–901.

Yu, H., B. Guo, S. Hanafy, F.-C. Lin, G. T. Schuster, et al., 2014, Direct detection of near-surface faults by migration of back-scattered surfacewaves: Presented at the 2014 SEG Annual Meeting, Society of Exploration Geophysicists.

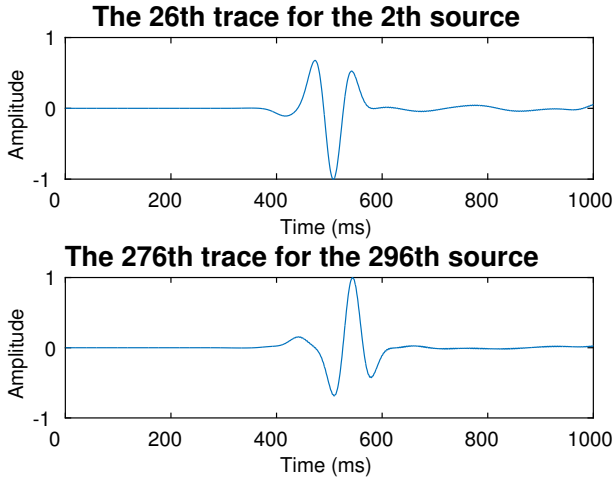

Figure 5: The backscattered records of two different source-receiver pairs by the model in figure 1: the location of source-receiver pair for the top one is on the left of the fault, and the location of the down one is on the right.

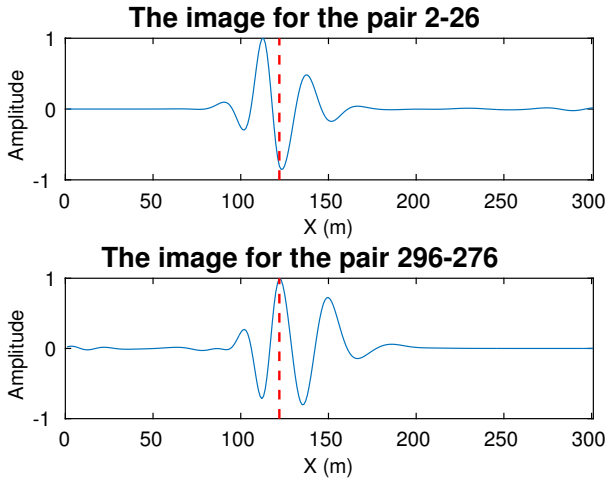

Figure 6: The NM images in my implement corresponding to the source-receiver pairs in figure 5, where red dash lines show the position of fault.